The kinematic properties of solar coronal mass ejections: Correction for projection effects in spacecraft coronagraph measurements

T. A. Howard[1], D. Nandy[1], and A. Koepke[2]

T. A. Howard (corresponding author), Department of Physics, Montana State University, Bozeman, MT, 59717. (thoward@physics.montana.edu)

[1]Department of Physics, Montana State University, Bozeman, MT, USA.

[2]West Virginia University, Morgantown, WV, USA.

Abstract.

One of the main sources of uncertainty in quantifying the kinematic properties of coronal mass ejections (CMEs) using coronagraphs is the fact that coronagraph images are projected into the sky plane, resulting in measurements which can differ significantly from their actual values. By identifying solar surface-source regions of CMEs using X-ray and Hα flare, and disappearing filament data, and through considerations of CME trajectories in 3D geometry, we have devised a methodology to correct for the projection effect. We outline this method here. The methodology was automated and applied to over 10000 CMEs in the CDAW (SOHO LASCO) catalog spanning 1996–2005, in which we could associate 1961 CMEs with an appropriate surface event. In the latter subset, de-projected speeds, accelerations and launch angles were determined to study CME kinematics. Our analysis of this subset of events reconfirms some important trends – notably that previously uncovered solar cycle variation of CME properties are preserved, CMEs with greater width have higher speeds and that slower CMEs tend to accelerate while faster CMEs tend to decelerate. This points out that statistical trends in CME properties – recovered from plane-of-sky measurements – may be preserved even in the face of more sophisticated 3D measurements from spacecrafts such as STEREO, if CME trajectories are predominantly radial. However, our results also show that the magnitude of corrected measurements can differ significantly from the projected plane-of-sky measurements on a case-by-case basis and that acceleration is more sensitive to the de-projection process than speed. Average corrected speed and acceleration tend to be a factor of 1.7 and 4.4 higher than their projected values, with mean corrected speed and acceleration magnitudes being on the order of 1000 km/s and 50 m/s^2, respectively. We conclude that while using the plane-of-sky measurements may be suitable for studies of general trends in a large sample of events,

1. Introduction

Coronal mass ejections (CMEs) are large-scale (often several 10's of degrees of heliospheric latitude) and massive (of the order of 10^{12} kg [e.g. *Harrison et al.*, 2003]) eruptions of plasma from the Sun, probably having their origin in solar photospheric and atmospheric magnetic field dynamics [e.g. *Zhang and Low*, 2005; *Nandy et al.*, 2007]. From an intellectual viewpoint they are of interest to the scientific community because they are mechanisms which allow for the removal of large amounts of magnetic flux and helicity from the Sun [*Low*, 1996] and are fundamental to the understanding of how magnetic energy is built-up, stored and released in magnetic flux systems. From a technological viewpoint they are of interest because they are believed to be responsible for major geomagnetic disturbances at Earth, contributing to severe space weather effects. These so-called geomagnetic storms are initiated when an interplanetary CME impacts with the Earth's magnetosphere, causing an enhancement of its ring current and aurora [e.g. *Dungey*, 1961]. A variety of damaging effects at Earth can result, including radiation hazards to polar air-traffic, disruption of electric power-grids and telecommunication facilities.

CMEs are observed by coronagraphs, which block out the main body of light from the Sun to reveal the faint surrounding corona. The largest, almost continuous database of observed CMEs assembled to date is from the Large Angle Spectroscopic Coronagraph (LASCO) [*Brueckner et al.*, 1995] instrument onboard the SOHO spacecraft. This instrument has the capacity to observe CMEs across a distance range of $\sim 2 - 30$ $R_\odot$ with a cadence of around 30-50 minutes. During the period of 1996 to 2005 a total of 10512 CMEs were cataloged and their central position angle (PA), angular width, speed,

acceleration, mass and kinetic energy recorded. The "SOHO LASCO CME Catalog" is available online at http://cdaw.gsfc.nasa.gov/CME_list/ and a survey of the data from this catalog up to 2002 has been published [*Yashiro et al.*, 2004]. This catalog has been used extensively in CME research, has been widely cited and is now generally accepted as a "first step" for those seeking to identify CMEs in a given time range or location, and study their kinematic properties.

In a statistical survey of the properties of CMEs listed in the catalog, *Yashiro et al.* [2004] demonstrated the variation of CME properties throughout the rising stage of the solar cycle. They investigated over 7000 cataloged CMEs and produced histograms showing the distribution of apparent (sky plane projected) width, latitude and speed in yearly intervals from 1996 to 2002, and acceleration in intervals of speed, from the slow ($\leq$ 250 km/s) to the fast ($>$ 900 km/s). They found that the number of narrow (apparent width $\leq 20^{\circ}$) CMEs increased as solar maximum approached and CME latitudes were localized around the equator at solar minimum. They also found a weak positive correlation between CME speed and width, and a tendency for fast CMEs to decelerate and slow CMEs to accelerate. This tendency was also identified in a later study of Earth-directed CMEs and associated shocks measured by the ACE spacecraft [*Howard and Tappin*, 2005]. Other statistical evaluations of CMEs and their properties have also been reported in the literature [e.g. *St. Cyr et al.*, 2000; *Vourlidas et al.*, 2002; *Gopalswamy et al.*, 2004].

It is to be noted that the data provided in the "SOHO LASCO CME Catalog" are often used without question and perceived as a quantitatively accurate measurement of the observed properties of CMEs. Such a practice may compromise the value of scientific studies due to the following limitations of the instrument and catalog:

1. Measurements are made at a single position angle or CME feature only, and different kinematic values are known to result from measurements made at different locations [e.g. *Robbrecht and Berghmans*, 2004; *Howard et al.*, 2006].

2. The definition of a CME is somewhat subjective [*Robbrecht and Berghmans*, 2004].

3. Multiple eruptions are often treated as a single eruption.

4. Some CMEs, particularly those known as halo CMEs [*Howard et al.*, 1982], are often associated with a brighter, non-halo component. Measurements tend to be made with the non-halo component, which can deviate from the halo component [*Howard et al.*, 2006].

5. Although CMEs are intrinsically 3-D structures [*Cremades and Bothmer*, 2004] and they propagate in 3-D space, all measurements are sky-plane projected, so kinematic (distance, speed and acceleration) properties can differ significantly from their true (3D) values, an effect that becomes more pronounced for CMEs originating away from the limb [see e.g. *Hundhausen*, 1993]. Moreover, the actual CME mass is different from the mass calculated based on sky-plane projected parameters.

Note that although Items 1-4 are important, they are not easily addressed unless changes are made in the CME identification and subsequent data reduction procedure itself [*Robbrecht and Berghmans*, 2004]. In this paper, we investigate the influence of Item 5, i.e. the projection effects on measurements documented in the "CDAW LASCO CME Catalog". This is possible by associating the CDAW CMEs (covering 1996–2005) with solar surface eruption events. We associated 1961 cataloged CMEs with either an X-Ray or Hα flare or a disappearing filament, and utilized their heliospheric coordinates to estimate the 3D direction of propagation of the CME. This allowed the calculation of the corrected (de-projected) speed and acceleration for each of the 1961 events, assuming that

CMEs propagate radially. In Section 2 we present the general methodology for correcting for projection effects in plane-of-sky measurements of CME kinematics (i.e., related to distance, speed and acceleration). We also discuss how corrections to projected mass measurements can be attempted (although, as discussed later, this cannot be done with information contained in the CDAW database). In Section 3 we outline the datasets (and their sources) that were used in this study. We present our analysis of the corrected CME kinematic properties in Section 4 and conclude with a discussion in Section 5. Our main results indicate that while statistical trends determined from sky-plane projected measurements are preserved in the corrected CME kinematic properties, individual values (of e.g. distance, speed or acceleration) can differ significantly between the projected and corrected parameters of any CME.

2. A Methodology for De-Projection of CME Kinematic Properties Based on 3D Geometry Considerations

All measurements made from coronagraph images are projected into the sky plane. In the case of LASCO, measured distances in solar radii are actually measurements of elongation ϵ, i.e. the angle between the Sun-Earth line and the line from the Earth to the measured point P. Elongation is converted to distance with the application of two assumptions:

- Light from P is Thomson scattered such that the line from the Earth to P is at right angles to the line from the Sun to P [e.g. *Vourlidas and Howard*, 2006]. This is known as the Point P approximation [e.g. *Howard et al.*, 2006]. Under this approximation, $R \sim \sin\epsilon$, where R is the distance from the Sun to P in units of AU.

- Elongation angles are small, such that $\sin\epsilon \sim \epsilon$, and hence $R \sim \epsilon$.

Therefore, for conversion of elongation angle to distance in solar radii, one simply takes ϵ in radians and multiplies by 1 AU in units of $R_\odot$, or $R \sim 216\epsilon$. This is the procedure applied for each distance measurement made using the LASCO analysis software.

2.1. Distance, Velocity & Acceleration

For the full 3D treatment, it is necessary to return to elongation measurements. Figure 1 shows an arbitrary point P (corresponding to a CME feature location) in a Heliocentric Earth-Ecliptic coordinate system [following *Howard et al.*, 2007]. An example of a CME associated with a Hα filament is given to demonstrate the association between the LASCO CME and the surface feature (Figure 1a). The Sun, S is at the center and the Earth, E lies on the x-axis 1 AU away. The z-axis is perpendicular to the plane of the Earth's orbit around the Sun (positive north). P is arbitrarily located a distance R away from the Sun on a sphere centered at S with radius R. Q is the projection of P onto the x-y plane and θ and ϕ are the co-latitude and longitude of the vector SP, relative to the Sun-Earth line. The elongation ϵ is $\angle$SEP and α is the angle subtended by P at the Sun, or $\angle$ESP. In terms of θ and ϕ,

$$\cos\alpha = \sin\theta\cos\phi. \tag{1}$$

Both ϵ and α are in the SEP plane. Using trigonometric considerations and the general 3D geometry depicted in Figure 1b we arrive at

$$\frac{1}{R} = \sin\alpha\cot\epsilon + \sin\theta\cos\phi. \tag{2}$$

Hence, with latitude, longitude and elongation information, we can determine the de-projected distance of any arbitrary point from the Sun [*Howard et al.*, 2007]. We obtain the longitude from the associated surface event. For each CME measurement, the central

PA was converted to solar latitude, which was used in preference to the latitude of the surface flare-event. This is because flares are more commonly associated with only one footpoint of the CME and therefore it may not be a true indicator of the "central-latitude" of the whole CME structure. The elongation was determined from the LASCO distance measurements.

Differentiating Equation (2) wrt time and assuming that CMEs propagate radially, we obtain

$$V_{3D} = \frac{dR}{dt} = R^2 \sin\alpha \mathrm{cosec}^2\epsilon \frac{d\epsilon}{dt}, \tag{3}$$

and

$$A_{3D} = \frac{d^2R}{dt^2} = \frac{V_{3D}}{d\epsilon/dt}\left(\frac{d^2\epsilon}{dt^2}\right) + 2V_{3D}\left[\frac{V_{3D}}{R} - \cot\epsilon\left(\frac{d\epsilon}{dt}\right)\right], \tag{4}$$

where

$$\frac{d\epsilon}{dt} = V_0 \sec\epsilon, \tag{5}$$

and

$$\frac{d^2\epsilon}{dt^2} = A_0 \sec\epsilon + V_0^2 \tan\epsilon \sec^2\epsilon. \tag{6}$$

Here, V_{3D} and A_{3D} are the de-projected speed and acceleration respectively, and V_0 and A_0 are the sky-plane projected speed and acceleration obtained from the catalog. These de-projected parameters, calculated based on the aforementioned 3D geometry considerations, are henceforth referred to simply as corrected (speed or acceleration) for ease of exposition.

2.2. Mass Determination

The determination of mass in the "CDAW SOHO LASCO Catalog" is based on the assumption that the mass of the CME is localized in the plane of the sky and that the integrated line of sight intensity is equal to the CME intensity at the point P being measured. LASCO CME mass is estimated using measurements of the brightness of the CME and the theory of Thomson scattering. Thomson-scattered white light from the Sun is maximized when the observer-P vector is orthogonal to the Sun-P vector (e.g. in the plane of the sky for a limb CME), and when this is not the case only a component of the scattered light at P is observed. This is described by *Billings* [1966] and involves the following, known as the Van de Hulst coefficients [*Van de Hulst*, 1950]:

$$A(R) = \cos\Omega \sin^2\Omega \tag{7}$$

$$B(R) = -\frac{1}{8}\left[1 - 3\sin^2\Omega - \cos^2\Omega\left(\frac{1+3\sin^2\Omega}{\sin\Omega}\right)\ln\left(\frac{1+\sin\Omega}{\cos\Omega}\right)\right] \tag{8}$$

$$C(R) = \frac{4}{3} - \cos\Omega - \frac{\cos^3\Omega}{3} \tag{9}$$

$$D(R) = -\frac{1}{8}\left[5 + \sin^2\Omega - \cos^2\Omega\left(\frac{5-\sin^2\Omega}{\sin\Omega}\right)\ln\left(\frac{1+\sin\Omega}{\cos\Omega}\right)\right], \tag{10}$$

where $\sin\Omega = \cos\Theta/R_0$ and Θ is the angle of the line SP to the plane of the sky. For a sky plane assumption, $\Theta = 0$ and $\sin\Omega = 1/R_0$. CME mass m is calculated by measuring the integrated intensity across a selected area on a running difference image B_{obs} through the following relation [*Vourlidas et al.*, 2000]:

$$m = \frac{B_{obs}}{B_e(\Theta)} \times 1.97 \times 10^{-27} \text{ kg}. \tag{11}$$

Here, $B_e(\Theta)$, known as the Thomson scattering function, is given by:

$$B_e(\Theta) = \frac{\sigma\pi}{2}[2(C + u(D-C)) - \cos^2\Theta(A + u(B-A))], \tag{12}$$

where σ is the scattering cross section, 7.95×10^{-26} per steradian and u accounts for limb darkening, $u = 063$. Mass measurements are therefore strongly dependent on angle Θ but a direct relationship between $m(\Theta)$ and $m(0)$ cannot be determined. To correct for projection in the mass measurements it is necessary to repeat the measurements made for the catalog with the same value of B_{obs} but with Θ equal to the direction of propagation of the CME. Without knowledge of the original value of B_{obs}, correction for mass is an intractable problem and therefore we do not attempt it here.

2.3. Procedure

With the previously discussed derivations we may now devise a technique for the de-projection of the measurements made in the CME catalog. For implementing this, the following procedure was adopted for the present study:

1. Read in the time of first appearance, PA, width, speed and acceleration data for each of the 10512 CMEs listed in the CDAW catalog.

2. Estimate the onset time (at solar surface) of each CME by assuming a constant speed radial propagation and projecting back to a certain distance from the measured location ($3R_\odot$ if LASCO C2 data are present, $6R_\odot$ if C3 data only are used).

3. Associate all flares and disappearing filaments (henceforth referred to as surface events) with a given CME when they satisfy both of the following criteria:

- The start time of the surface event is within one hour either side of the onset time (from Item 2) of the CME, to account for the assumption of constant speed for calculating the onset time.

• The heliospheric latitude and longitude are in the same quadrant as any part of the angular span of the CME.

4. Given the projected speed, acceleration (V_0 and A_0) and central position angle from the catalog, the co-latitude θ and longitude ϕ of the associated surface events (determined by using Items 1-3 above), determine the corrected speed and acceleration by using Equations (3) and (4) respectively.

5. Create a new list with all the projected CME parameters along with the corrected ones, including the details of each associated surface event. Some CMEs were found to be associated with more than one surface event, in which case the corrected CME parameters based on each surface event are listed.

3. Datasets

Along with the LASCO data listed in the CME catalog, it was necessary to identify a source region for the CMEs. This is currently best achieved by searching for solar surface events which occur around the right time and sector of the Sun as the CME onset. For the present study we have selected surface events for which extensive catalogs are maintained. These include X-Ray flare data provided by the GOES spacecraft and ground-based Hα flare and disappearing filament data. The relationship between flares, filaments and CMEs has been known since the discovery of CMEs [*Howard et al.*, 1975; *Munro et al.*, 1979; *Dryer*, 1982]. The lists of these events were obtained from the Solar Geophysical Database. From 2001 onwards, Soft X-Ray Imager (SXI) data onboard GOES-12 allows the identification of the location of X-Ray flares on the solar surface. Complementary to

this, data are available from ground-based Hα observatories for the entire period of the study.

4. Results

Our database of deprojected CME kinematic parameters contains the original CME data (date, time, PA, width, projected speed and acceleration) along with CME onset time, corrected speed and acceleration, the time range of the surface event, its location and type. For those events where there is more than one associated surface event, all are listed. Of the 10512 cataloged CMEs we identified 1961 events for which there was at least one associated surface event. This represents only 19% of the CME data set and is close to the value of 28% (260 out of 938) obtained by including C class flares into the halo CME results of *Howard and Tappin* [2005]. This reinforces the claim that the vast majority of CMEs are not associated with a flare or disappearing filament, albeit with the understanding that some associated surface events could have been overlooked (either not recorded or not uncovered by our selection process).

Variations in CME PA and associated surface event locations (the latter from our database) over the solar cycle are demonstrated in Figure 2. The central position angle of each CME has been converted to a relative latitude following *Yashiro et al.* [2004]. Figure 2a shows the distribution of all 10512 CMEs in the LASCO catalog plotted with time. During the rising and declining stages of the solar cycle there is a tendency for events to become localized around the equatorial region but the tendency is much stronger in the rising stage (1996-1999). *Yashiro et al.* [2004] cited this as due to CME location tending to localize around the heliospheric current sheet which also tends to be near the equator around solar minimum. During solar maximum there is an even spread of CME location

from equator to pole. This tendency is preserved when we consider only those events for which we have a surface event, as shown in Figure 2b. Finally, Figure 2c shows the distribution of the location in solar latitude of the inferred surface events with time. Given that most of the surface events are solar flares, possibly associated with solar ARs, it is not surprising that this assumes the form of a Maunder Butterfly Diagram. Addition of high-latitude filament associated CME data can plausibly generate a poleward branch in this CME butterfly diagram [see e.g. *Cremades et al.*, 2006].

To compare the general solar cycle trends in the corrected speed and acceleration to earlier results, Figures 3 and 4 show the variation of these parameters, following the same format as *Yashiro et al.* [2004]. The speed measurements are separated into yearly plots and acceleration into plots representing speed ranges, from the low to the high. In both cases the number of CMEs in each plot is given and the average speed is shown in Figure 3. In each case panel a) shows the apparent parameter and panel b) the corrected. From Figure 3 it appears that the general trends are preserved in the projection removal process, with distributions remarkably similar between the apparent and corrected parameters, albeit with larger mean and variance for the corrected values. Even increases and decreases from year to year are preserved (e.g. there is an increase in event number from 2001 to 2002 and an increase in average speed from 2002 to 2003 in both apparent and corrected cases). For acceleration (Figure 4), the distribution again appears largely unaffected by projection removal, aside from a larger variance for the corrected cases. An important earlier result, notably that slower CMEs tend to accelerate and faster CMEs tend to de-accelerate is also evident in the distribution of the corrected CME accelerations. Nonetheless, there are significant quantitative differences. Half of the CMEs had corrected speeds which

were within 5% of the apparent speed, but 4% of CMEs had corrected speeds which were more than twice the apparent speed. For acceleration, the differences were larger, with half of the CMEs having corrected acceleration within 20% of the apparent values, but 15% of the CMEs had corrected acceleration which were more than twice the apparent acceleration.

We now turn to a critical examination of the relationship between corrected and apparent CME parameters. Figure 5 shows the relationship between corrected and apparent speed and acceleration, respectively. The line $y = x$ (dashed line) would result if corrected and apparent values were equal. In several cases it is clear that the corrected and apparent parameters lie close to the $y = x$ line. However, both apparent speed and acceleration represent only the lower threshold (in magnitude) of the actual (corrected) values. We perform a statistical analysis to highlight the differences between the corrected and apparent parameters to a greater detail. To negate the influence of statistical outliers, corrected speeds in excess of 7000 km/s and corrected acceleration with magnitudes greater than 800 m/s^2 were removed from this analysis (there were about 10 such cases). Table 1 summarizes the differences in statistical descriptors of the corrected and apparent parameter distributions – the mean, standard deviation (representing the scatter in the distribution), maximum and minimum values are depicted. The differences are significant; e.g. the mean corrected speed exceeds the mean apparent speed by a factor of 1.7, while the mean corrected acceleration is opposite in sign to the apparent and exceeds the latter by a factor of 4.4. The scatter and range of the corrected parameters are larger than the apparent parameters, with a significant number of CMEs exceeding speeds of 4000 km/s (the upper limit for apparent speed) and acceleration magnitudes of 500 m/s^2.

A statistical correlation analysis between the corrected and apparent speeds (Figure 5-left) generated a Pearson's linear correlation coefficient of 0.71 and a Spearman's rank correlation coefficient of 0.78, both exceeding 99.99% confidence levels. Although the relationship is strongly positive, given that the correlation coefficient based on the distribution of ranks is higher than the linear correlation coefficient, the relationship between the corrected and apparent speed is possibly non-linear. This, in conjunction with the large scatter in corrected values, given any apparent value (which is due to the fact that CMEs with the same apparent speed, but originating in different solar locations, can have a wide range of corrected speeds), precludes the possibility of any simple relationship existing between the corrected and apparent values. The same arguments hold for the relationship between apparent and corrected acceleration (Figure 5-right), for which, the recovered Pearson's linear correlation coefficient is 0.76 and the Spearman's rank correlation coefficient is 0.86 (again, both exceeding 99.99% confidence levels).

Figure 6 shows the distribution of apparent (left) and corrected (right) speeds plotted as a function of apparent CME width W. In this plot, only non-halo CMEs with widths less than 360° are considered. The relationship in this case is predominantly linear, with apparent speeds versus width having a Pearson's linear correlation coefficient of 0.19 and corrected speeds versus width having a Pearson's linear correlation coefficient of 0.13 (both at 99.99% confidence levels). Therefore, the general trend between corrected speed and width is consistent with that between apparent speed and width, namely that CMEs with higher width have greater speeds; this supports the results of *Yashiro et al.* [2004]. The (least-squares) linear fit to the distribution is also shown in Figure 6 and it is found that the positive linear trend is stronger for the corrected speed versus width distribution.

Finally, we explore the effect of CME source-region location on plane-of-sky projected parameters and the factor by which it needs to be corrected. Based on the theory of correction for projection effects (outlined in Section 2) and the accompanying 3D CME trajectory geometry depicted in Figure 1, it is obvious that the plane-of-sky projection affects the determination of CME speeds and acceleration most when the event originates at solar disk-center (for events originating at or near the limb, the apparent parameters are a fairly good approximation for the actual values). This is confirmed in Figure 7 where we plot the ratio of corrected to apparent speed versus CME source-region longitude (left) and the ratio of corrected to apparent acceleration versus CME source-region longitude (right). Clearly, the correction factor is greatest for events located near disk-center (i.e., longitude = 0°), while the correction factor approaches unity at solar limb (longitude = 90°). Therefore, correcting for projection effects is crucial for CMEs which originate at or near disk-center, if one has to get a better handle on the magnitudes of its kinematic properties.

5. Discussion

The objective of the present study was to correct for plane-of-sky projection effects on coronagraph measurements of CME kinematics and analyze the resulting kinematic properties (note that intrinsic data limitations as outlined in points 1–4 in Section 1 still apply to our analysis). The results show that general solar cycle trends in CME kinematics appear to be preserved after the de-projection process. Our conclusions based on these trends therefore are in agreement with the earlier study of *Yashiro et al.* [2004], who analyzed the catalog of plane-of-sky projected CME kinematic properties. Specifically, the trends are that CME location tends to be localized about the equator during solar

minimum and CME speed increases near solar maximum. CMEs with lower speeds tend to accelerate while those with higher speeds tend to decelerate. Physically this suggests that many CMEs occur near the heliospheric current sheet and change their speed through interactions with the ambient solar wind. We also find that CMEs with greater width have higher corrected speeds. Our results and comparative analysis suggest that these general trends may be recovered even in the more sophisticated 3D measurement of CME trajectories that are to be expected from the STEREO spacecraft – especially if the pragmatic assumption of radial CME trajectories is confirmed.

For the majority of events, the differences between projected and measured speeds was not large. However, it is clear that some events were much faster than what the apparent speeds suggested, and a small number were more than 10 times the value. These events suffer maximum projection effects and are very close to the Sun-Earth line (originating near solar disk-center). Acceleration appears to be more sensitive to projection effects, as 15% of all events had corrected accelerations larger than twice the apparent values. These results demonstrate the necessity to consider projection effects on a case-by-case basis for studies where a numerically precise determination of its kinematic properties is warranted. These results also support the conclusions of earlier studies of projection effects based on limb CME measurements from the Solar Maximum Mission [*Burkepile et al.*, 2004] and halo CME measurements from the LASCO instrument [*Michalek et al.*, 2003].

The fastest projected speed for a CME was 3387 km/s, cataloged for the halo CME on 10 November 2004. This is one of only two CMEs with a projected speed >3000 km/s. There are many events, however, with corrected speeds >3000 km/s, and some

with speeds >5000 km/s. Flight times between 0 and 1 AU for Earth-directed CMEs suggest an average speed much lower than this [e.g. *Howard and Tappin*, 2005]. Such travel times would still be expected as these extremely fast CMEs would be expected to slow down greatly on passage to 1 AU (for comparison, the LASCO field of view on which our analysis is based, covers barely over a tenth of the Sun-Earth distance). For example, the CME on 6 November 2004 at 08:06 UT has a corrected speed of 5651 km/s and an acceleration of –577 m/s^2. Near the Sun, our analysis suggests new upper limits of CME speeds and accelerations, at ∼7000 km/s and ∼800 m/s^2, respectively.

The nature of the instrument leads to a bias toward faster events for those with a large component along the Sun-Earth line. Slow events tend to be missed by running difference image sequences because if any part of the CME in the present image is overlayed by the CME in the previous image it will be subtracted away. Hence there will be a bias toward faster CMEs. Our results indicate that correction factors for speeds and acceleration tend to be higher near disk center. This is due to the fact that CMEs which originate near disk center have a larger component on the Sun-Earth line. This results in apparent (projected) speed estimates that may be significantly lower than the intrinsic (true) speed. Due to the projection effect, the ratio of the radial distance travelled to the projected distance travelled, increases as one moves from limb to disk center; accounting for the latter results in a higher correction factor. Running differences will also tend to miss these relatively slower CMEs.

We point out that the usage of associated surface events may introduce a source of error in the present work. Firstly, there is not a one-to-one correspondence between CME and flare location as flares are localized at a particular region of the Sun while CMEs often

span several 10's of degrees of solar latitude. Flares also have a tendency to occur at one footprint of the CME, as suggested by the difference in trends between Figures 2b and c. Hence, as an approximate correction, we have applied the assumption that CME latitude is that of the central position angle, but the longitude is that of the surface event. Even considering that some errors arise because of this assumption, the differences in statistical properties of CME kinematics between the corrected and apparent (projected) parameters (as evident in Table 1) are significant enough to argue that these differences ought not to be taken lightly. We expect that 3D observations with STEREO will confirm this.

Acknowledgments. We acknowledge helpful discussions with Hebe Cremades, Nat Gopalswamy and David Webb. SOHO is a project of international cooperation between ESA and NASA, and the SOHO/LASCO catalogs are maintained by NASA, The Catholic University of America and the US Naval Research Laboratory (NRL). They are made available courtesy of Goddard Space Flight Center and NRL. The Solar Geophysical Database is maintained by NOAA and made available courtesy of the Solar-Terrestrial Physics Division. This research was supported in parts by NASA Grants NNG06GA37G, NNG05GE47G and NSF grant ATM-0603789. Support was also provided by a NSF Research Experience for Undergraduates (REU) Program Grant ATM-0243923 to Montana State University.

References

Billings, D. E., *A Guide to the Solar Corona*, New York Academic Press, 1966.

Brueckner, G. E., R. A. Howard, M. J. Koomen, C. M. Korendyke, D. J. Michels, J. D. Moses, D. G. Socker, K. P. Dere, P. L. Lamy, A. llebaria, M. V. Bout, G. M. Simnett,

D. K. Bedford and C. J. Eyles, The Large Angle Spectroscopic Coronagraph, *Solar Phys. 162*, 357, 1995.

Burkepile, J. T., A. J. Hundhausen, A. L. Stanger, O. C. St. Cyr and J. A. Seiden, Role of projection effects on solar coronal mass ejection properties: 1. A study of CMEs associated with limb activity, in *J. Geophys. Res.,109*, A03103, 2004.

Cremades, H. and V. Bothmer, On the three-dimensional configuration of coronal mass ejections, *Astron. Astrophys. 422*, 307, 2004.

Cremades, H. and V. Bothmer and D. Tripathi, Properties of structured coronal mass ejections in solar cycle 23, *Adv. Space Res. 38*, 461, 2006.

Dryer, M., Coronal Transient Phenomena, *Space Sci. Rev., 33*, 233, 1982.

Dungey, J. W., Interplanetary Magnetic Field and the Auroral Zones, *Phys. Rev. Lett., 6*, 47, 1961.

Gopalswamy, N., S. Nunes, S. Yashiro and R. A. Howard, Variability of solar eruptions during cycle 23, in *Adv. Space Res., 34*, 391, 2004.

Harrison, R. A., P. Bryans, G. M. Simnett and M. Lyons, Coronal dimming and the coronal mass ejection onset, *Astron. Astrophys. 400*, 1071, 2003.

Howard, R. A., M. J. Koomen, D. J. Michels, R. Tousey, C. R. Detwiler, D. E. Robers, R. T. Seal, J. D. Whitney, R. T. Hansen, S. F. Hansen, C. J. Garcia and E. Yasukawa, Synoptic Observations of the Solar, in *WDC-A Report UAG-48, NOAA, Boulder*, 1975.

Howard, R. A., D. J. Michels, N. R. Sheeley Jr. and M. J. Koomen, The observation of a coronal transient directed at Earth, *Astrophys. J., 263*, L101, 1982.

Howard, T. A. and S. J. Tappin, Statistical survey of earthbound interplanetary shocks, associated coronal mass ejections and their space weather consequences, *Astron. Astro-*

phys., 440, 373, 2005.

Howard, T. A., C. D. Fry, J. C. Johnston and D. F. Webb, On the evolution of interplanetary coronal mass ejections in interplanetary space, *Astrophys. J.*, Submitted, 2007.

Howard, T. A., D. F. Webb, S. J. Tappin, D. R. Mizuno, and J. C. Johnston, Tracking halo coronal mass ejections from 0-1 AU and space weather forecasting using the Solar Mass Ejection Imager (SMEI), *J. Geophys. Res., 111*, A04105, doi:10.1029/2005JA011349, 2006.

Hundhausen, A. J., Sizes and locations of coronal mass ejections - SMM observations from 1980 and 1984-1989, *J. Geophys. Res., 98*, 13177, 1993.

Low, B. C., Solar activity and the Corona, *Solar Phys. 167*, 217, 1996.

Michalek, G., N. Gopalswamy and S. Yashiro, A New Method for Estimating Widths, Velocities, and Source Location of Halo Coronal Mass Ejections, *Astrophys. J., 584*, 472, 2003.

Munro, R. H., J. T. Gosling, E. Hildner, R. M. MacQueen, A. I. Poland and C. L. Ross, The association of coronal mass ejection transients with other forms of solar activity, *Solar Phys., 61*, 201, 1979.

Nandy, D., D. H. Mackay, R. C. Canfield and P. C. H. Martens, Twisted solar active region magnetic fields as drivers of space weather: Observational and theoretical investigations, *J. Atmos. Solar Terr. Phys.*, in press, 2007.

St. Cyr, O. C., R. A. Howard, N. R. Sheeley Jr., S. P. Plunkett, D. J. Michels, S. E. Paswaters, M. J. Koomen, G. M. Simnett, B. J. Thompson, J. B. Gurman, R. Schwenn, D. F. Webb, E. Hildner and P. L. Lamy, Properties of coronal mass ejections: SOHO LASCO observations from January 1996 to June 1998, *J. Geophys. Res., 105*, 18169,

2000.

Robbrecht, E. and D. Berghmans, Automated recognition of coronal mass ejections (CMEs) in near-real-time data, *Astron. Astrophys. 425*, 1097, 2004.

Van de Hulst, H. C., The electron density of the solar corona, *Bull. Astron. Inst. Neth., 11*, 135, 1950.

Vourlidas, A., D. Buzasi, R. A. Howard and E. Esfandari, Mass and energy properties of LASCO CMEs, in Solar variability: from core to outer frontiers, Wilson, A. (ed.), *ESA SP-506, 1*, Noordwijk: ESA Publications Division, 91, 2002.

Vourlidas, A. and R. A. Howard, The proper treatment of coronal mass ejection brightness: A new methodology and implications and observations, *Astrophys. J., 642*, 1216, 2006.

Vourlidas, A., P. Subramanian, K. P. Dere and R. A. Howard, Large-angle spectrometric coronagraph measurements of the energetics of coronal mass ejections, *Astrophys. J., 534*, 456, 2000.

Yashiro, S., N. Gopalswamy, G. Michalek, O. C. St. Cyr, S. P. Plunckett and R. A. Howard, A catalog of white light coronal mass ejections observed by the SOHO spacecraft, *J. Geophys. Res., 109*, doi:10.1029/2003JA010282, 2004.

Zhang, M. and B. C. Low, The hydromagnetic nature of solar coronal mass ejections, *Annu. Rev. Astron. Astrophys., 43*, 103, 2005.

Table 1. Difference in statistical properties of the apparent and corrected, speed and acceleration datasets. The values in boldface represent mean of the absolute value of acceleration.

Parameter	Mean	Std. Dev.	Maximum	Minimum
Apparent Speed (km/s)	571.13	363.79	3387.00	26.00
Corrected Speed (km/s)	993.67	796.40	6591.10	40.10
Apparent Acceleration (m/s^2)	3.05 (**18.24**)	36.43	434.80	-96.70
Correction Acceleration (m/s^2)	-13.37 (**40.37**)	81.37	749.27	-751.10

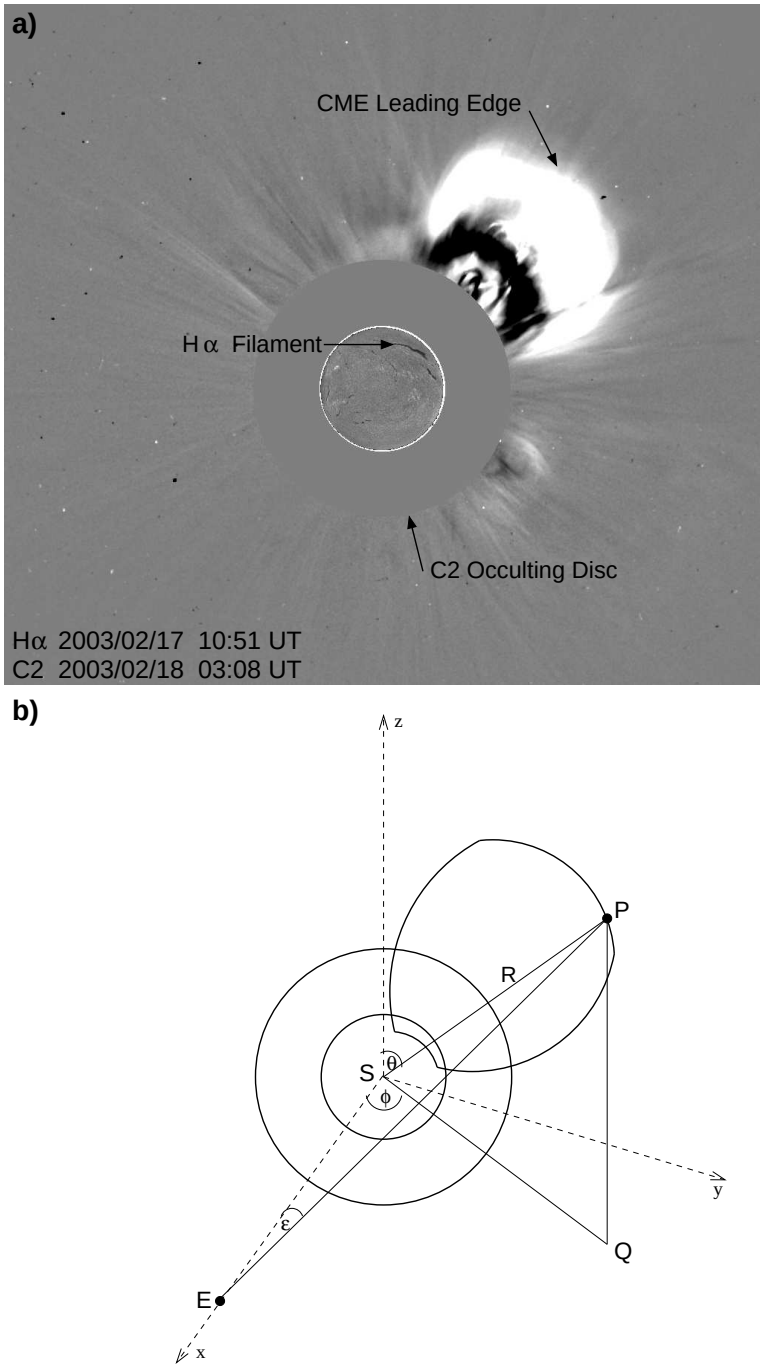

Figure 1. a) A LASCO C2 image with a Hα image superimposed. The LASCO image was taken on 2003/02/18 at 03:08 UT and contains a bright CME to the north west. The associated filament is shown in the Hα image taken the day before, on 2003/02/17 at 10:51 UT. b) A schematic diagram of the image in (a) with the associated geometry overlayed. The Sun, S, Earth, E and measured point P are shown along with the elongation ϵ, co-latitude θ and longitude ϕ. The distance SP is given as R [*Howard et al.*, 2007].

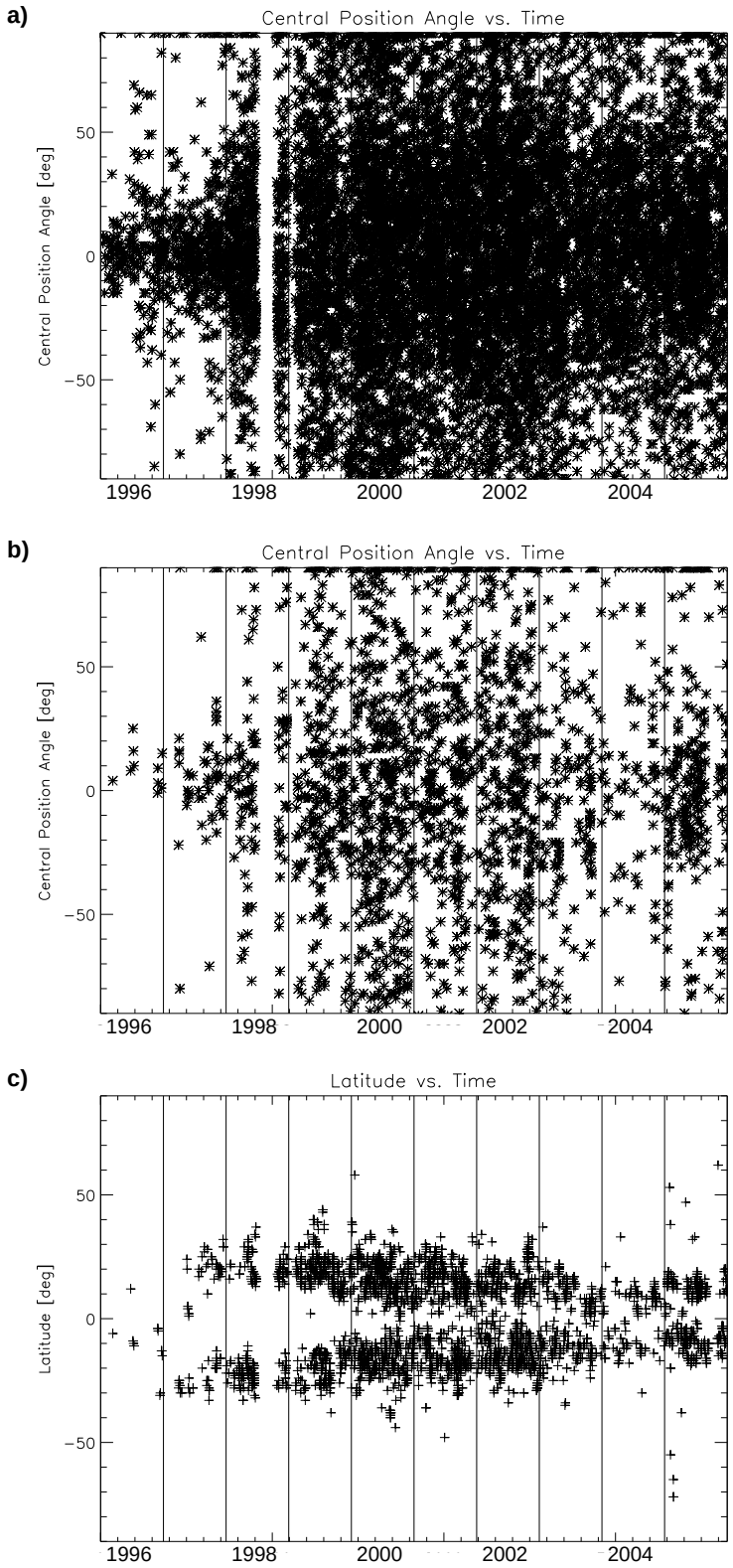

Figure 2. a) Central position angle, converted to latitude, plotted against time for each of the 10512 events. b) CME PA (latitude) for the 1961 "surface" associated events, plotted against time. c) Surface event latitude vs time for the 1961 "surface" associated events.

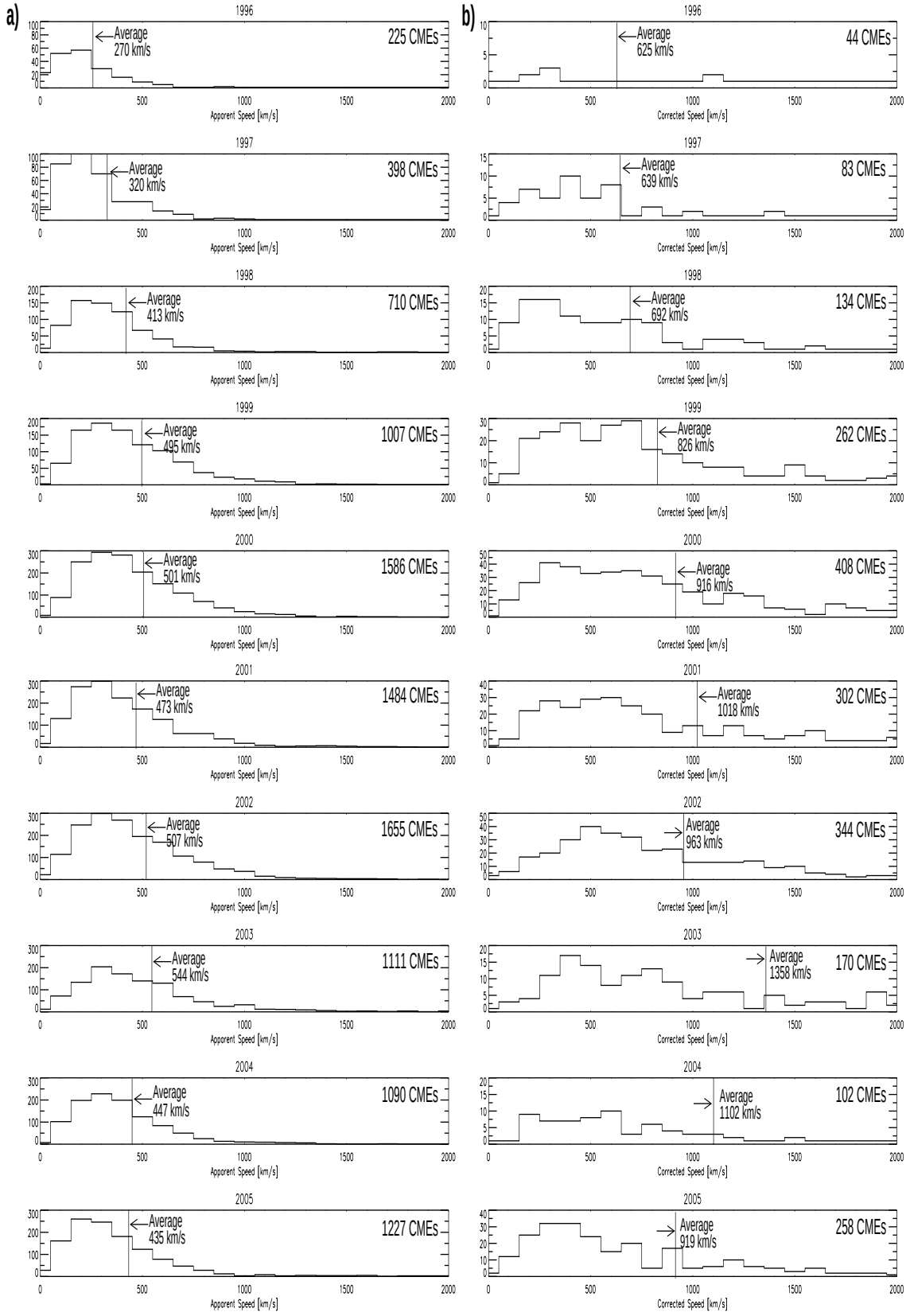

Figure 3. a) Apparent and b) corrected speed distributions for each year from 1996-2005. The number of events and average speed is given for each year.

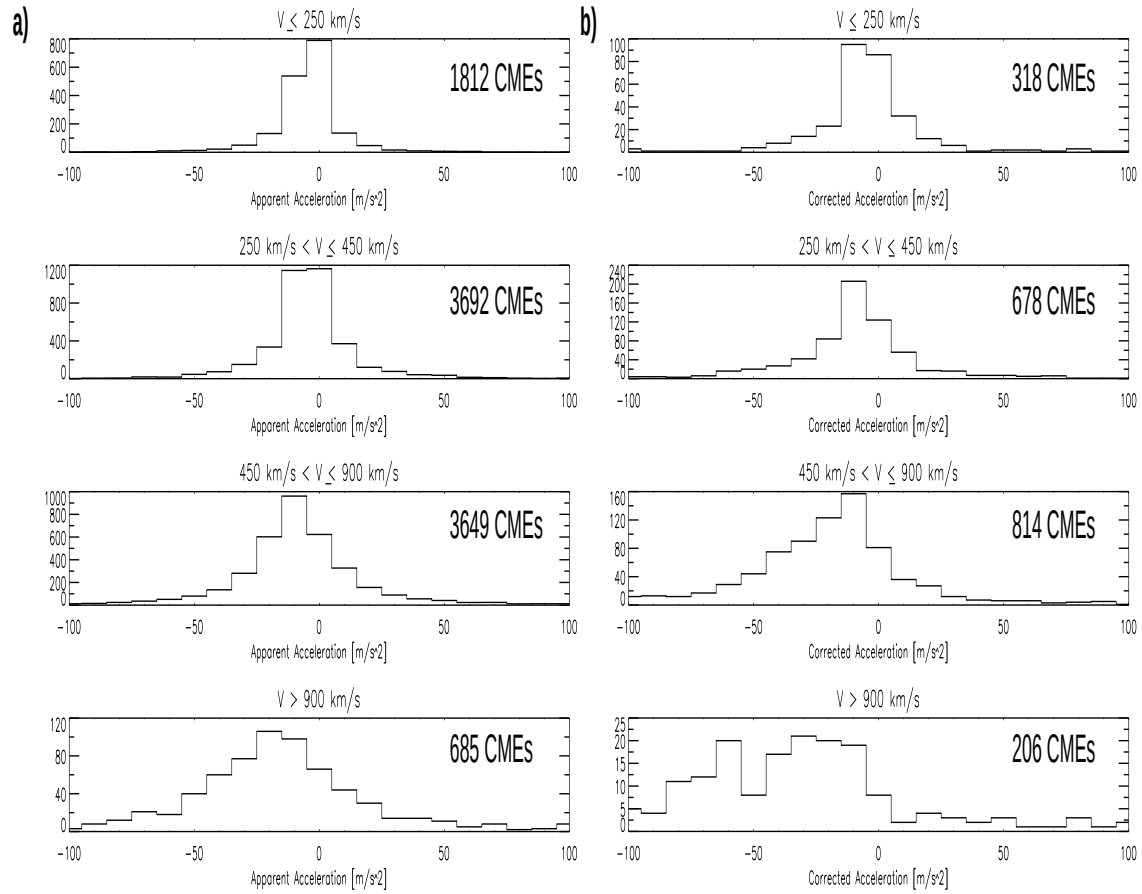

Figure 4. a) Apparent and b) corrected acceleration distributions in separate plots representing the range of CME speeds from $V \leq 250$km/s, 250 km/s $< V \leq 450$ km/s, 450 km/s $< V \leq 900$ km/s, and $V > 900$ km/s. The number is events in each case is given.

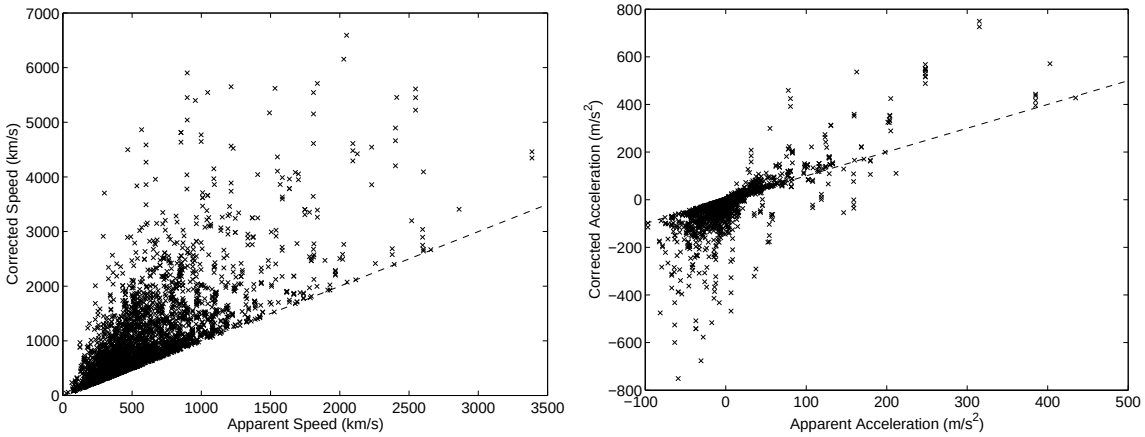

Figure 5. Corrected versus apparent speed (left) and acceleration (right). The dashed $y = x$ line would result if the corrected and apparent parameters were equal

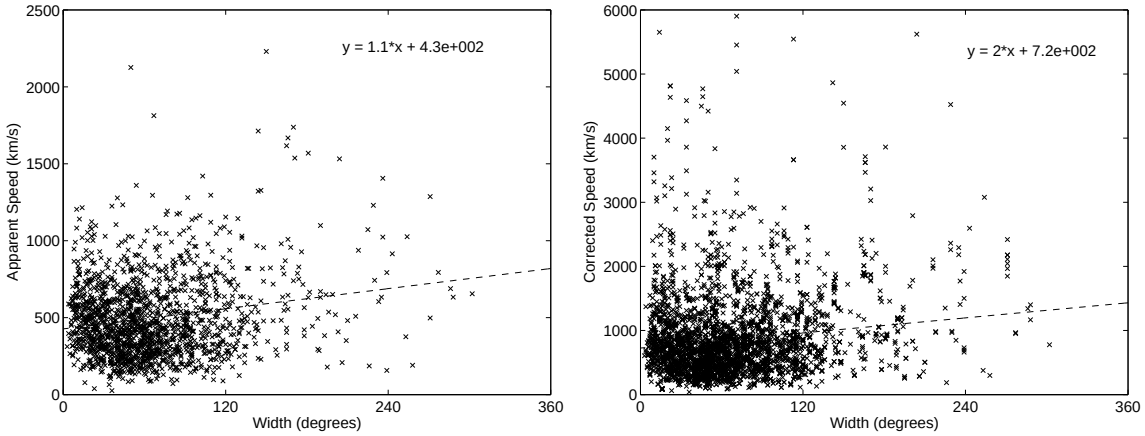

Figure 6. Apparent (left) and corrected (right) speed as a function of apparent width. In both cases the dashed line depicts the linear fit; the linear trend is stronger in the corrected speed versus width distribution.

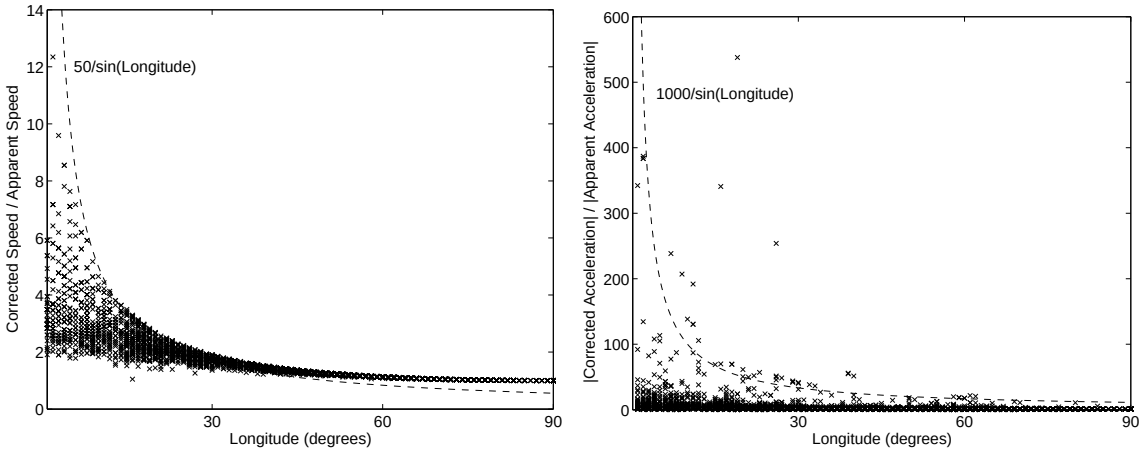

Figure 7. The ratio of corrected to apparent speed (left) and corrected to apparent (absolute value of) acceleration (right) versus CME source-region longitude. The dashed line, depicting a 1/sin(longitude) trend seems to capture the behavior of the data. However, we advise against the usage of this simple relationship for correction because the exact correction factor varies on a case by case basis – which is obvious from the scatter.